Research Article Vol. 3, No. 1 / 15 January 2020 / OSA Continuum 10

Microspherical nanoscopy: is it a reliable technique?

RADU MALUREANU,[1,*] OSAMU TAKAYAMA,[1] EVGENIY SHKONDIN,[1,2] ANDREY NOVITSKY,[1,3] AND ANDREI V. LAVRINENKO[1]

[1] *Department of Photonics Engineering, Technical University of Denmark, 2800 Kgs. Lyngby, Denmark*
[2] *Currently with the National Centre for Nano Fabrication and Characterization, 2800 Kgs. Lyngby, Denmark*
[3] *Currently with the Department of Theoretical Physics and Astrophysics, Belarusian State University, Nezavisimosti Avenue 4, 220030 Minsk, Belarus*
[*] *rmal@dtu.dk*

Abstract: We looked at the typical resolution provided by microspheres in nanoobject imaging. The resolution was studied with two kinds of materials: high-index barium titanate glass and low-index polystyrene. Spheres of different sizes were taken, and thus we also checked if there is any dependence of the resolution capabilities on their dimensions. We concluded that, although we observed an increase in resolution for some of the spheres, practical considerations and lack of consistency in imaging makes this technique too cumbersome for practical applications.

1. Introduction

The imaging beyond the notorious diffraction limit [1] is the never-ending quest. The latest update on the nomenclature of the methods allowing for sub-diffraction and even deeply sub-diffraction imaging is quite pronounced including such techniques as STED [2], STORM [3], confocal [4] or interference (SLIM) [5] microscopy. Nevertheless, ideas of explicit visualization of objects features less than $\lambda/2$ without any additional steps, labeling, expensive and/or bulky equipment are remarkably appealing. Thus, there are plenty of publications reporting on breaking the $\lambda/2$ constrain by simple means [6].

The nanoscopy enabled by microspheres has emerged quite recently [7–9]. Since then the resolution of features with sizes below the diffraction limit has been reported routinely. However, achieving of $\lambda/6 - \lambda/8$ resolution requires additional objects been involved, for example, plasmonic particles, wires and gratings [9–11]. Instead, labeling of small objects with fluorescent molecules can also greatly enhance resolution [12,13]. Some authors even claim resolution of minimal features down to $\lambda/17$. A table summarizing the state-of-the-art in resolution of nanosized features with microspheres in different configurations can be found in recent paper by Maslov & Astratov [14].

The thrilling point in the microspheres-based nanoscopy is that, so far, no rigorous theory behind such resolution exists. As clearly illustrated in [14], the photonics nanojets theory cannot explain such high numbers of exceeding the diffraction limit. Pure geometrical optics approach is not capable of letting the resolution step out this limit too. Therefore, the complete theory is still waiting to be developed. Thus far, any new experimental data and observations in applications of microspheres (MSs) to enhance the optical resolution should be considered as important preliminary steps in the basement of such theory.

We employed two kinds of spheres from barium titanate glass (BTG, n = 1.95) and from polystyrene (PS, n = 1.59) with several different sizes in order to study the influence of spheres' refractive index. BTG microspheres with various diameters ranging from 2 μm to 150 μm have been used as high refractive index spheres in liquid immersion. [9,15–23] While such exhaustive range may provide insight into the functioning of the structures, the different approaches used

#378355 https://doi.org/10.1364/OSAC.378355
Journal © 2020 Received 4 Oct 2019; revised 11 Dec 2019; accepted 11 Dec 2019; published 20 Dec 2019

OSA CONTINUUM

make such analysis cumbersome. However, it should be noted that, in some cases, there is a clear dependency of the magnification with particle size [9,16] while in other cases this correlation does not seem to exist [15]. Furthermore, in some papers, they state that there should be no correlation between the spheres' dimension and the magnification [7]. The experimental magnification factor in [15] can vary from 2.5 to 4, irrespective of the sphere diameter. Such large variation is similar to the one we see in our case, even if our microspheres are much smaller. Also in the case where a correlation between magnification and particle size is present, like for example in [9], if we restrict the data in the range of the particles we used, it can be seen that the magnification values are quite scattered, thus making difficult any interpretation.

Also in our case, the spheres with diameters of 12–24 μm for BTG spheres and 10–30 μm for PS spheres were always fully immersed in the liquid (water). No other special arrangements were undertaken; no other routines besides just straight imaging through the spheres and a microscope objective were applied. Therefore our conclusions are limited to the fully immersed, coaxial illumination experiments and do not include other geometries, like inclined incidence [21] or half-immersed [24] ones. We tried to find a reliable procedure in order to characterize the magnification of the MSs and the improvement compared to standard microscopy. By "standard microscopy" we mean imaging with a 100× magnification (NA = 0.95) objective, in white unpolarized light and the bright field mode.

The organization of this article is as in the following. Fabrication of the samples and parameters of the spheres are described in Section 2. Images of the features obtained by different MSs are presented in Section 3. Post-processing of the images and analysis of results are contained in Section 4. Conclusions end the article in Section 5.

2. Parameters of the samples and the microspheres

The samples for the probing of resolution are arrays of Au disks deposited on a silicon wafer in a square lattice as shown in Fig. 1. The Au thickness is 80 nm. The lattice period varies between 150 and 500 nm with 50 nm steps. To prepare samples we used electron beam lithography (EBL). Accordingly to estimations by the geometrical optics approach [15], and experiments with the Blu-ray disks [22], we have in our disposal samples which theoretically can be resolved by both BTG and PS spheres (pitch sizes 450-500 nm), samples which can be resolved with BTG spheres only (pitch 250-400 nm) and completely unresolved samples (pitch 150-200 nm).

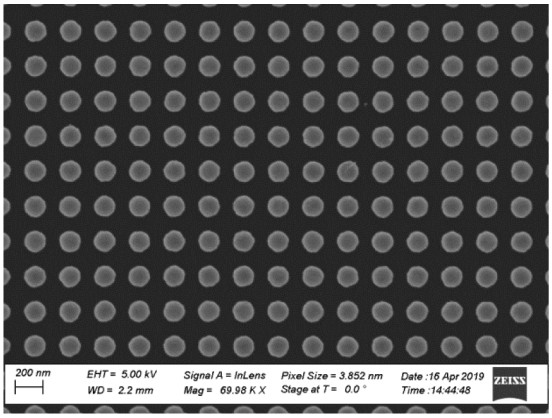

Fig. 1. SEM image of a typical 250 nm period lattice.

We decided to use periodic structures since, in this case, the image analysis is much more consistent through the use of Fourier transforms. Although mathematical procedures for analyzing

OSA CONTINUUM

individual object rather than periodic structures are in place [25], they are not as widespread as the ones analyzing periodic structures. We are confident that our structures do not pose problems in imaging through the existence of diffraction orders of the evanescent waves [26]. In this case, the authors base their functioning on the amplification of evanescent waves through a negative index slab. We have no such slab and therefore the evanescent waves decay exponentially from the structure. Furthermore, we image the grating itself, not use the grating to image a different structure. Also, since the largest period investigated (300 nm) is smaller than the smallest imaging wavelength (380 nm [27]), our structures do not have propagating first order diffraction order. Therefore the image we see is of the grating, not an interference pattern.

As it was already stated we used two sets of MSs: high-index BTG spheres with radii varying between 6 and 12 μm, and PS spheres with radii 5, 10, and 15 μm. Also, we used the spheres either in air or immersed in water. As such we have 4 systems: BTG in air, BTG in water, PS in air and PS in water. Out of those, we could not image for the the BTG in air and the PS in water systems. We believe this to be due to the interplay between the field of view and the index contrast. The BTG in air have a huge index contrast but that generates a very low field of view and major spherical aberrations. Thus, this system was unreliable. In the case of PS in water, the index contrast is only 1.19, therefore the image contrast was too low to be above the noise level and we could not see any lattice image. For PS in air, we could obtain very low contrast images of the lattice. However, in this case, when trying to enhance the image contrast digitally using blind deconvolution (see below), we completely removed the grating image. We thus reached the conclusion that the contrast in the obtained images is too low for reliable processing. The most reliable system is the BTG in water one, where the index contrast is 1.47. In the following, we refer only to this system.

As a baseline, in Fig. 2 we show 500 nm and 300 nm lattices imaged directly with a microscope objective in the same conditions. The 500 nm lattice can be clearly seen (Fig. 2(a)), but not the 300 nm one (Fig. 2(b)). Apart from the images themselves, their Fourier transforms (in the insets) clearly show peaks in the case of 500 nm lattice and their absence in the case of the 300 nm one. It should be noted that the zero order peak is clearly visible in the center of the Fourier transform images.

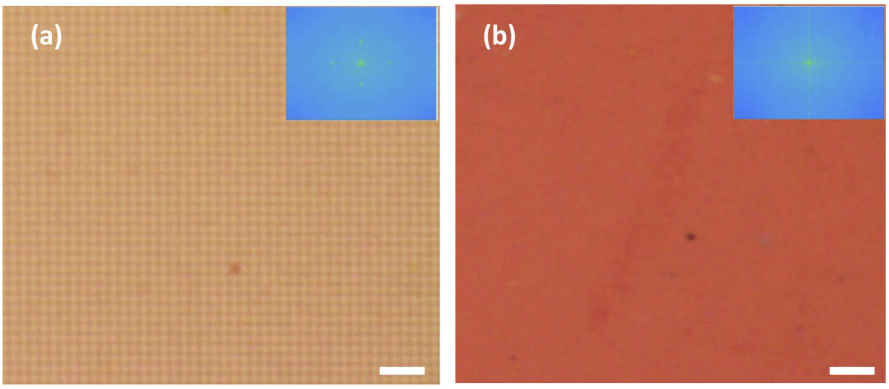

Fig. 2. Optical microscope image (100× magnification, NA = 0.95 objective) of a 500 nm (a) and 300 nm (b) period lattices, taken in air. In the insets, the Fourier transforms of the images showing the clear presence of the grating (a) and its absence (b). The scalebars are 2.5 μm.

OSA CONTINUUM

3. Analysis of images

Using the BTG spheres in water, the lowest period we managed to image was 250 nm. The twice improvement in resolution came at the cost of lower contrast. Apart from this, there are several other issues that worth being mentioned. The imaging procedure consists of acquiring frames at various "imaging planes", under the sample surface. Due to restrictions on the microscope stage, the actual imaging plane level cannot be measured. However, the step between one imaging plane and another was kept roughly constant. Using the microscope stage, we tried, for each separate experiment, to keep the step in the propagation direction constant. The procedure for this was to first determine where the first image of the grating appears. Then, we moved back a slam but controllable amount and took one image. We then continued to take images after each step forward until there were no images of the gratings. Since we cannot measure the stage movement, using this procedure was the only way to ensure at least that the step between one imaging plane and the next is constant. Due to this limitation, we generally looked for clusters of spheres with various dimensions such that we can better compare the images obtained from them. In general, the clusters contained between 6 and 9 spheres with radii between 6 and 12 μm. A typical image of a 250 nm lattice in such cluster is shown in Fig. 3.

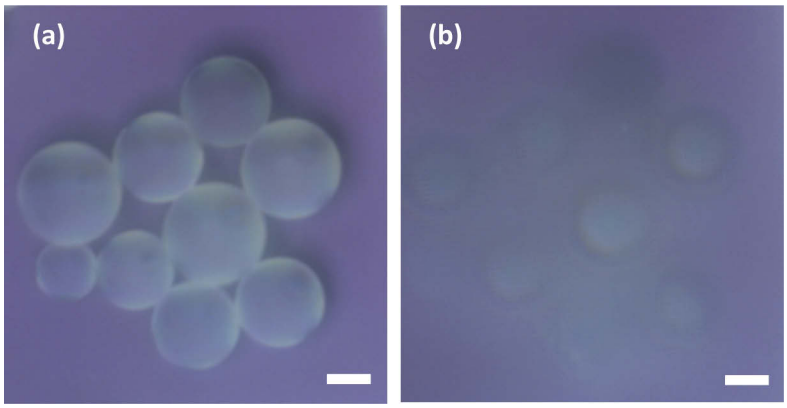

Fig. 3. Optical microscope image of a cluster of BTG spheres used for imaging (a) and a 250 nm lattice viewed through them (b). It can be seen that some spheres image the lattice while others do not. The scalebars are 10 μm.

It can be seen that some spheres (out of focus) show lattice images while others do not. Each of these images (between 6 and 9 for each cluster) is then divided into several sets, each corresponding to a specific sphere. A typical cropped image of one sphere looks like the one in Fig. 4.

While one can guess if there is a lattice imaged there, it is obvious that the lack of contrast makes the analysis of such image cumbersome. To improve the contrast, the first step is to make an iterative blind deconvolution with an initial guess of the point spread function (PSF) [28–30]. In our case, for all the images, the initial guess of the PSF was a uniform one over the whole image area. The deconvoluted image now appears to be similar to the ones in the first two panels of Fig. 5.

It can be seen that the lattice in the first panel (Fig. 5(a)) is much clearer now in comparison with Fig. 4. The areas where the lattice is imaged are clearly differentiated from the ones where there is no lattice at all. This, corroborated to the initial image and to the fact that there is no lattice after deconvoluting images where we could not see faint patterns before (Fig. 5(b)), give us the confidence that the lattice image is not a spurious result of deconvolution. However, one can clearly see deconvolution artifacts as high-frequency lattices in the image.

OSA CONTINUUM

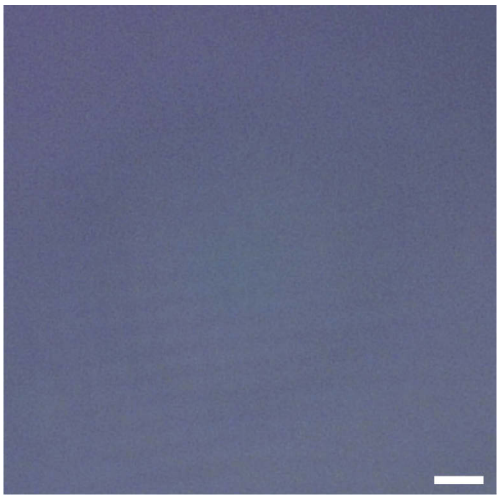

Fig. 4. Crop of a lattice image from a specific sphere. These cropped images were then used for processing. The scalebar is 1 μm

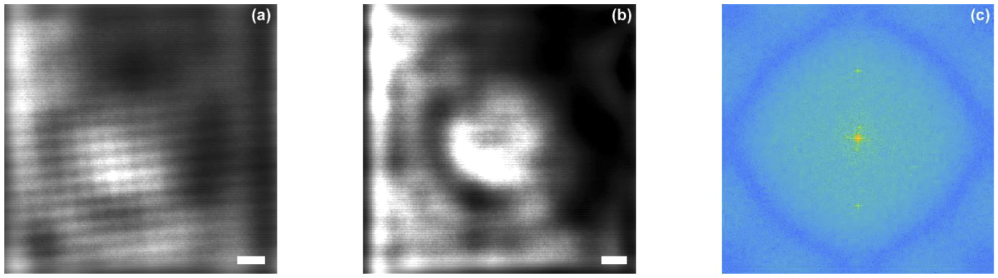

Fig. 5. (a) Typical image of a lattice after deconvolution. It shows a much higher contrast as well as areas where there is no lattice imaged. (b) Typical image when a lattice was not imaged. A high-frequency periodicity can be observed as an artifact of the deconvolution. (c) The Fourier transform of an image with lattice present. Apart from the 0-order peak, in the center of the figure, one can see 4 maxima, close to the center, related to the lattice period and two more, related to artifacts in the deconvolution. The scalebars are 1 μm

Once the deconvolution is done, the image is then Fourier transformed, thus obtaining the k-space (Fig. 5(c)). The peaks in the Fourier transform allow us to quantify the period of the lattice. Also, in the Fourier transform image, the deconvolution artifacts can be easily identified as peaks further away from the center. To calculate the lattice period and the magnification of the sphere, the following algorithm was performed:

1. We found the positions of two of the maxima in the FFT spectra, ignoring the zero-order peak and the remote ones introduced by deconvolution
2. We calculated the length L (in pixels) of the line that passes through the peaks and reaches the border of the image
3. We calculated the distance d, in pixels, between the two maxima
4. The period of the lattice is then calculated as $P = 2 \times \frac{L}{d} \times \mathrm{p/M}_o$ where p is the physical pixel size of the CCD camera while M_o is the magnification of the microscope objective.

OSA CONTINUUM

5. The obtained magnification from the sphere is then $M = P/\Lambda$ where Λ is the real lattice period.

We then imaged the spheres themselves and measured their radius such that we can correlate the focus depth with the dimension of the spheres. Due to the error in measuring the sphere dimensions, we rounded them up to the nearest integer.

We performed this procedure for clusters formed on both 250 and 300 nm lattices. We chose these periods as limiting cases since the lattices with periods lower than 250 nm could not be imaged while the ones with periods above 300 nm can surely be imaged. The results are presented in Fig. 6. Each panel shows a different cluster of BTG spheres from the same batch. The first two panels show results for the 250 nm period lattice, different clusters, while the last panel is for the 300 nm lattice. The lines imply the same sphere images the lattice at different planes.

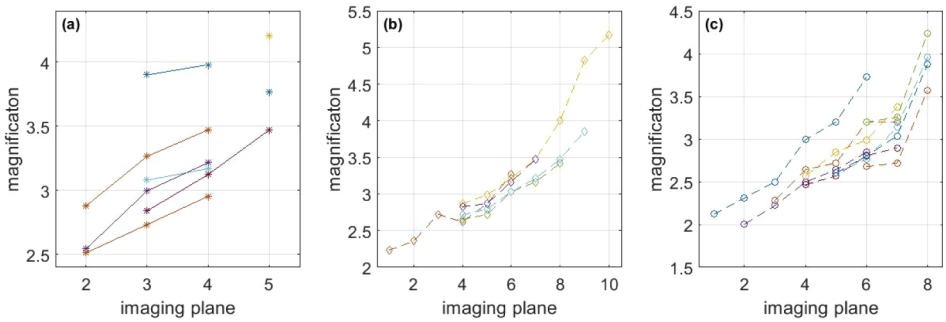

Fig. 6. The variation of the magnification function of the imaging plane, for the spheres that allowed viewing the lattices. It can be seen that magnification can vary substantially for the same sphere. The panels are for different sphere clusters. (a) and (b) are lattices with 250 nm period while (c) is a lattice with 300 nm period. The same convention will be kept throughout the subsequent images. To be noted that the "imaging plane" number cannot be correlated from one graph to another.

It can be clearly seen that some spheres image the lattices for a wide range of planes while others have only one imaging plane. Also, there are spheres that cannot image the lattices at any plane (not shown). Apart from these exceptions, there is a clear tendency of increasing the magnification while imaging farther from the surface. Still, from here we can already see that it is difficult to assign a certain magnification for a sphere, without imposing extra conditions. On

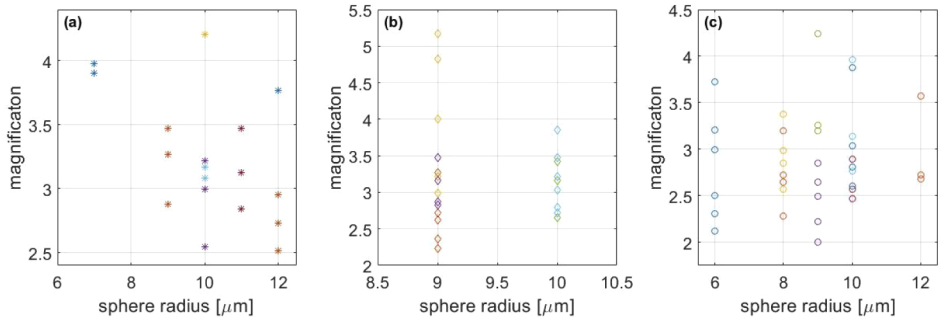

Fig. 7. The variation of magnification function on the sphere radii in micrometers. It clearly shows that the spheres with the same radius can image with different magnifications. Each sphere is denoted with one specific color to differentiate between the variation within one sphere and the variation from one sphere to another, but having the same radius.

OSA CONTINUUM

the other hand, if we try to correlate the radius of the sphere with the magnification, the results are even less straightforward (Fig. 7).

It can be seen that for the same radius of the sphere, the magnification can vary wildly, in some cases even with a factor of 2 or more. However, it should be noted that in this image are shown all the magnifications that a sphere can provide. Still, there is no evidence of direct dependence of magnification on the radius of the microspheres [7]. A clear example can be seen in Fig. 7(a) for the 10 μm spheres. One sphere images the lattice only in one plane and has a 4.25× magnification, another in two planes and has an average magnification of 3.15 while a third has a images in three planes and has a magnification between 2.55 and 3.25. Such inconsistency between the expected values of magnification and the observed ones were also reported in the literature [14,15,17].

A third correlation that we tried to establish is between the sphere radius and the focusing level or plane-of-focus position [14]. In this case, the classical ray optics formulae tell us that the focal length of a sphere is given by $f = n \times R/(2 \times (n-1))$ [7,31] where n is the relative refractive index and R is the radius of the sphere. In our case, the relative refractive index is 1.47, so $f \cong 1.6 * R$. Applying the lens equation [31] and assuming the lattice is touching the bottom part of the sphere meaning the source plane is at distance R from the lens, we obtain that the image plane is formed at 2.5 times the radius of the sphere, counting it from the sphere center. Since our focusing levels are related more to the level of the lattice, the imaging plane is about 1.5 times the radius of the sphere. In any case, it should theoretically manifest a clear linear dependency on the spheres radius. The figure below (Fig. 8) shows the experimental values for the position of the imaging plane. In the case of several clear images for the same sphere, the focus level is taken as the average value.

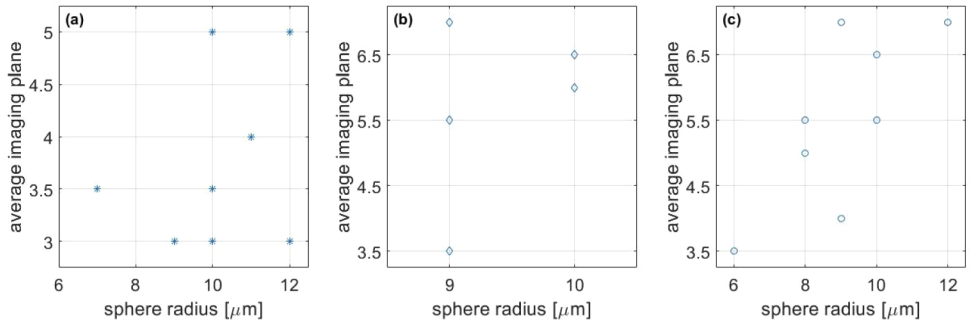

Fig. 8. The average depth of the imaging plane function of the sphere radii in micrometers. According to the ray optic theory, position of the imaging plane should be linearly dependent on the sphere radii, the fact that cannot be experimentally verified.

It can be clearly seen that there is hardly any correlation between the average focus level and the sphere dimensions. Especially when considering that different spheres with the same radius have different imaging planes, even if the images were taken in the same conditions. Since the theory behind the functioning of the microspheres for resolution-enhancement is not clear, we cannot state the reasoning behind this discrepancy.

In order to double-check the results, we applied the same procedure for a 50× magnification. Also in this case, there is no clear connection between the sphere radius and the average imaging plane (Fig. 9), or magnification (Fig. 10). However, the same tendency between the imaging plane and magnification was observed (Fig. 11).

OSA CONTINUUM

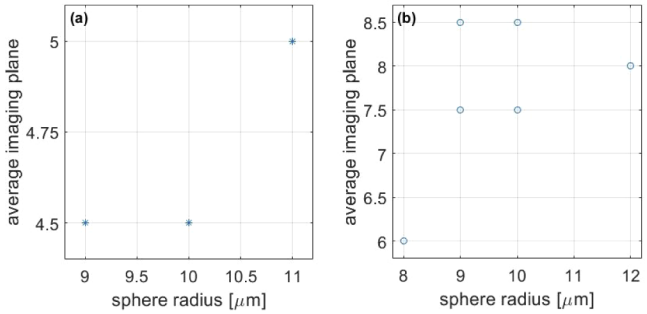

Fig. 9. The average depth of the imaging plane function of the sphere radii in micrometers in the case of a 50× magnification objective. Also in this case, there is no clear correlation between the imaging plane and the sphere radii. (a) is for 250 nm lattice period and (b) is for 300 nm lattice period. This convention is kept for the subsequent figures.

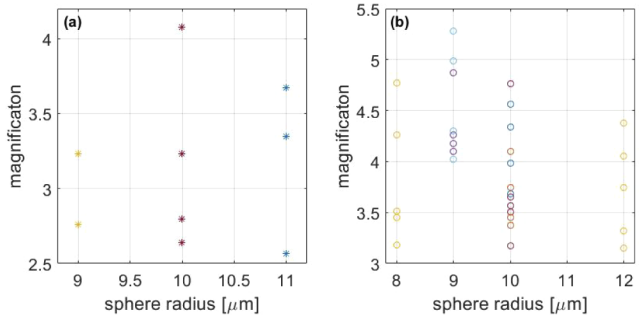

Fig. 10. The magnification function of the sphere radii in micrometers in the case of a 50× magnification objective. The same conclusion as from the 100× magnification objective applies.

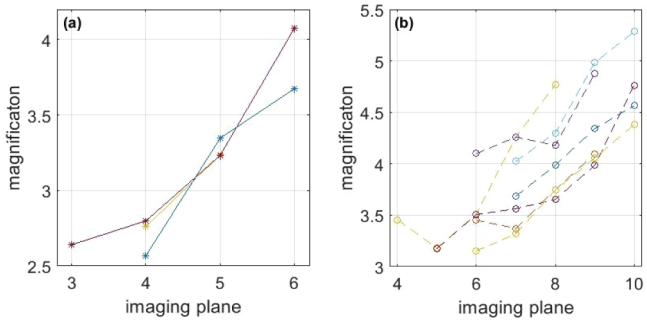

Fig. 11. The magnification function of the imaging plane in the case of a 50× magnification objective. Also here, a clear increase in magnification with depth is observed.

OSA CONTINUUM

4. Conclusion

During our experiments, the only correlation we could observe was between the imaging plane and magnification. As such, it seems that deeper under the substrate one images, bigger the magnification. Apart from this, there was no correlation between the size of the spheres and the magnification or the imaging plane. Furthermore, it seems that obtaining the magnified, higher resolution image is not related only to the refractive indices of the sphere and the surrounding and the sphere dimensions but also to other yet unknown factors. As such, spheres made with nominally identical materials with similar dimensions and in identical experimental conditions give different results in terms of magnification and resolution.

In conclusion, although dielectric microsphere-based systems may offer a two-fold enhancement of the resolution and a few to several times more additional magnification, the practical issues, like controlled positioning of the spheres, consistency within the image, lack of contrast etc. make this approach, in our opinion, challenging.

However, we would like to stress that this investigation was made for the simplest geometry, where the illumination is coaxial and the spheres are fully immersed. Therefore its conclusions cannot be directly applied to other arrangements. Also, with the development of the theory, the inconsistencies we found may be explained and the technique may become feasible.

Funding

Villum Fonden (11116).

Acknowledgments

The authors would like to acknowledge the support from the Danish National Center for Micro- and Nanofabrication (DTU Nanolab).

Disclosures

The authors declare no conflicts of interest and no commercial relationship related to the content of the manuscript.

References

1. M. Born and E. Wolf, *Principles of Optics: Electromagnetic Theory of Propagation, Interference and Diffraction of Light* (Cambridge University Press, 1999).
2. S. W. Hell and J. Wichmann, "Breaking the diffraction resolution limit by stimulated emission: stimulated-emission-depletion fluorescence microscopy," Opt. Lett. **19**(11), 780 (1994).
3. M. J. Rust, M. Bates, and X. Zhuang, "Sub-diffraction-limit imaging by stochastic optical reconstruction microscopy (STORM)," Nat. Methods **3**(10), 793–796 (2006).
4. R. H. Webb, "Confocal optical microscopy," Rep. Prog. Phys. **59**(3), 427–471 (1996).
5. Z. Wang, L. Millet, M. Mir, H. Ding, S. Unarunotai, J. Rogers, M. U. Gillette, and G. Popescu, "Spatial light interference microscopy (SLIM)," Opt. Express **19**(2), 1016 (2011).
6. S. So, M. Kim, D. Lee, D. M. Nguyen, and J. Rho, "Overcoming diffraction limit: From microscopy to nanoscopy," Appl. Spectrosc. Rev. **53**(2-4), 290–312 (2018).
7. Z. Wang, W. Guo, L. Li, B. Luk'yanchuk, A. Khan, Z. Liu, Z. Chen, and M. Hong, "Optical virtual imaging at 50 nm lateral resolution with a white-light nanoscope," Nat. Commun. **2**(1), 218 (2011).
8. G. Huszka and M. A. M. Gijs, "Turning a normal microscope into a super-resolution instrument using a scanning microlens array," Sci. Rep. **8**(1), 601 (2018).
9. A. Darafsheh, G. F. Walsh, L. Dal Negro, and V. N. Astratov, "Optical super-resolution by high-index liquid-immersed microspheres," Appl. Phys. Lett. **101**(14), 141128 (2012).
10. L. A. Krivitsky, J. J. Wang, Z. Wang, and B. Luk'yanchuk, "Locomotion of microspheres for super-resolution imaging," Sci. Rep. **3**(1), 3501 (2013).
11. Y. Yan, L. Li, C. Feng, W. Guo, S. Lee, and M. Hong, "Microsphere-Coupled Scanning Laser Confocal Nanoscope for Sub-Diffraction-Limited Imaging at 25 nm Lateral Resolution in the Visible Spectrum," ACS Nano **8**(2), 1809–1816 (2014).
12. A. Bezryadina, J. Li, J. Zhao, A. Kothambawala, J. Ponsetto, E. Huang, J. Wang, and Z. Liu, "Localized plasmonic structured illumination microscopy with an optically trapped microlens," Nanoscale **9**(39), 14907–14912 (2017).

OSA CONTINUUM

13. A. Brettin, F. Abolmaali, K. F. Blanchette, C. L. McGinnis, Y. E. Nesmelov, N. I. Limberopoulos, D. E. Walker, I. Anisimov, A. M. Urbas, L. Poffo, A. V. Maslov, and V. N. Astratov, "Enhancement of resolution in microspherical nanoscopy by coupling of fluorescent objects to plasmonic metasurfaces," Appl. Phys. Lett. **114**(13), 131101 (2019).
14. A. V. Maslov and V. N. Astratov, "Resolution and Reciprocity in Microspherical Nanoscopy: Point-Spread Function Versus Photonic Nanojets," Phys. Rev. Appl. **11**(6), 064004 (2019).
15. L. Li, W. Guo, Y. Yan, S. Lee, and T. Wang, "Label-free super-resolution imaging of adenoviruses by submerged microsphere optical nanoscopy," Light: Sci. Appl. **2**(9), e104 (2013).
16. H. Yang, R. Trouillon, G. Huszka, and M. A. M. Gijs, "Super-Resolution Imaging of a Dielectric Microsphere Is Governed by the Waist of Its Photonic Nanojet," Nano Lett. **16**(8), 4862–4870 (2016).
17. A. Darafsheh, N. I. Limberopoulos, J. S. Derov, D. E. Walker, and V. N. Astratov, "Advantages of microsphere-assisted super-resolution imaging technique over solid immersion lens and confocal microscopies," Appl. Phys. Lett. **104**(6), 061117 (2014).
18. A. Darafsheh, C. Guardiola, A. Palovcak, J. C. Finlay, and A. Cárabe, "Optical super-resolution imaging by high-index microspheres embedded in elastomers," Opt. Lett. **40**(1), 5 (2015).
19. A. Darafsheh, "Influence of the background medium on imaging performance of microsphere-assisted super-resolution microscopy," Opt. Lett. **42**(4), 735 (2017).
20. G. Huszka, H. Yang, and M. A. M. Gijs, "Microsphere-based super-resolution scanning optical microscope," Opt. Express **25**(13), 15079 (2017).
21. F. Wang, L. Liu, H. Yu, Y. Wen, P. Yu, Z. Liu, Y. Wang, and W. J. Li, "Scanning superlens microscopy for non-invasive large field-of-view visible light nanoscale imaging," Nat. Commun. **7**(1), 13748 (2016).
22. S. Gao, K. Meng, Z. Yang, H. Liu, T. Chen, and L. Sun, "Large field-of-view super-resolution image obtained by manipulating submerged microsphere," J. Phys.: Conf. Ser. **1074**, 012172 (2018).
23. J. W. Park, A. J. Pedraza, and W. R. Allen, "The interface between sputter-deposited gold thin films and ion-bombarded sapphire substrates," Appl. Surf. Sci. **103**(1), 39–48 (1996).
24. Y. E. Geints and A. A. Zemlyanov, "Photonic nanojet super-resolution in immersed ordered assembly of dielectric microspheres," J. Quant. Spectrosc. Radiat. Transfer **200**, 32–37 (2017).
25. K. W. Allen, Y. Li, and V. N. Astratov, "Reply to "Comment on 'Super-resolution microscopy by movable thin-films with embedded microspheres: Resolution analysis' [Ann. Phys. (Berlin) 527, 513 (2015)]," Ann. Phys. **528**(11-12), 901–904 (2016).
26. Z. Liu, S. Durant, H. Lee, Y. Pikus, N. Fang, Y. Xiong, C. Sun, and X. Zhang, "Far-Field Optical Superlens," Nano Lett. **7**(2), 403–408 (2007).
27. Wikipedia, "Visible spectrum," https://en.wikipedia.org/wiki/Visible_spectrum.
28. T. J. Holmes, D. Biggs, and A. Adu-Tarif, "Blind deconvolution," in *Handbook of Biological Confocal Microscopy*, J. B. Pawley, ed. (Plenum Press, 1995).
29. R. J. Hanisch, R. L. White, and R. L. Gilliland, "Deconvolutions of Hubble Space Telescope Images and Spectra," in *Deconvolution of Images and Spectra*, P. A. Jansson, ed., 2nd ed. (Academic press, 1997).
30. D. S. C. Biggs and M. Andrews, "Acceleration of iterative image restoration algorithms," Appl. Opt. **36**(8), 1766 (1997).
31. M. Sasaki, T. Kurosawa, and K. Hane, "Micro-objective manipulated with optical tweezers," Appl. Phys. Lett. **70**(6), 785–787 (1997).